ORIGINAL ARTICLE

A correlational study of process parameters on properties of low-pressure cold sprayed copper coatings

Maricruz Hernández-Hernández[1] · Rodrigo González-Mejía[2] · Victor Hugo Mercado-Lemus[1] · Adriana Gallegos-Melgar[1] · Isabel Pereyra[3] · Juan Muñoz-Saldaña[4] · Jan Mayén[3]

Abstract

Here, statistics descriptive and inferential were employed to understand the acquired data from the process output variables such as porosity percentage, thickness, and deposition efficiency of the obtained coatings as a function of process input variables such as nozzle type, standoff distance, and the particle in-flight velocity before impact on the substrate. Coatings were produced by the LPCS process with copper powder deposited onto aluminum 6061 substrates, using two different nozzle shapes (rectangular and round) and two standoff distances (SOD) of 12.5 and 22.5 mm. It was found that nozzle type is the process input parameter with the most substantial contribution to the final coating properties. Particle in-flight velocity decreased by 38% at the standoff distance of 22.5 mm with the rectangular nozzle shape. In contrast, at the same standoff distance for the round nozzle shape, the in-flight particle velocity only diminished by 15%. The rectangular nozzle exhibits the uppermost change of in-flight particle velocity, impacting the particles at a very high speed. This could cause a high percentage of rebounded particles, diminishing the thickness and increasing the porosity percent. It was concluded that the round nozzle type is recommended to achieve coatings with low porosity levels without deep dependence on the standoff distance. This conclusion applies to the experimental conditions of this study with the given geometrical nozzle features.

Keywords Cold spraying · Low-pressure cold spraying · Copper coatings · Inferential study · Statistical modeling

1 Introduction

Cold gas dynamic spraying (CGDS) is relatively the last technology developed in the spray additive manufacturing processes. CGDS offers several advantages over other traditional techniques since the particles are deposited in a solid-state by a kinetic energy source instead of the thermal energy used in conventional spraying techniques. The solid-state deposition method by using temperatures far below particle melting point in cold gas processes avoids inevitable defects associated with deposition methods by thermal energy such as high-temperature oxidation, evaporation, melting, residual thermal stress, or phase transformations, among others [1–4]. Another CGDS important advantage is a high deposition rate (DR) achieved, resulting in ultra-thick layers (5–50 mm) with high bond strength [2, 5]. These advantages allow CGDS the deposition of low melting and easily oxidable metal-based materials retaining their microstructure during deposition [6]. Industrial applications of cold spray processes are increasing daily in different industries such as aerospace, energy, automotive, and biotechnology, among several others [2, 3, 7, 8]. CGDS techniques emerged as a new alternative technique for coating deposition for enhancing the mechanical and physical properties of many components, as well as repairing and refurbishing critical components with a thickness of a few millimeters, making this technology an effective and cost-saving alternative to replacing expensive and worn out complex parts [1, 2].

✉ Maricruz Hernández-Hernández
salipi05@gmail.com; maricruz.hernandez@ciateq.mx

1 CONACYT-Corporación Mexicana de Investigación en Materiales, CP 25290 Saltillo, Coahuila, México

2 Facultad de Ciencias de la Ingeniería y Tecnología, Universidad Autónoma de Baja California, Unidad Valle de las Palmas, Blvd Universitario 1000, Unidad Valle de las Palmas, 22260 Tijuana, B.C, México

3 CONACYT-CIATEQ A.C., Centro de Tecnología Avanzada, Eje 126 No. 225, Zona Industrial, CP 78395 San Luis Potosí, SLP, México

4 Centro de Investigación y de Estudios Avanzados del I.P.N. Unidad Querétaro, Libramiento Norponiente 2000, 76230 Querétaro, México

The deposition process during CGDS starts with the acceleration of a jet of powder particles carried by a supersonic jet of a compressed gas (N2, He, or air). Powder particles (5–50 μm) achieve velocities from 300 to 1200 m/s at temperatures of up to 1000° C through a de Laval-type nozzle, a convergent-divergent device [9]. The particle velocity before the impact is typically between 500 and 800 m/s. After their impact, the particles are plastically deformed and adhere to the substrate located approximately 10–40 mm from the exit gun (called stand-off distance, SOD) [8, 10]. Particle adhesion is reached only if particle velocity impact is higher than critical velocity [11, 12], which is mainly a function of the properties of the material being deposited, as was reported by the research team that developed CGDS.

Critical velocity depends on particle properties. This value determines the impact behavior of the powder particles, which can deform and adhere to the surface under the total impact energy to form a coating, or powder particles can rebound diminishing deposition efficiency (DE) and other coatings properties [4, 13]. Deposition efficiency is defined by the weight gained from substrates after spraying divided by the product of the feeding powder rate and the spraying time. The powder particle impacting angle and its influence on deposition efficiency have also been studied [14]. The physical and mechanical substrate characteristics, as well as its temperature, can affect the critical velocity for achieving particle adhesion. Preheating the substrate modifies the material thermal behavior, increasing plastic behavior and softening the surface substrate, which increases bonding mechanisms driving particle adhesion [14]. The substrate surface roughness can also significantly enhance mechanical interlocking, offering more places to lodge the particles to the bonding as roughness increases.

CGDS processes are mainly divided into High-Pressure Cold spraying (HPCS) and Low- Pressure Cold spraying (LPCS). This division is determined by characteristics such as injection method powder into the nozzle, operational variable, and portability. HPCS is operated at high pressure and temperature of 25 to 30 bar and 1000 °C, respectively. This system feeds powder particles into de gas stream axially with N_2 or He as the gas propellant to achieve particle velocities between 400–1200 m/s [1–3, 15] and needs a high-pressure powder feeder to avoid powder backflow, which is expensive and large. On the other hand, LPCS operates at relatively low pressure (5–10 bar) by using compressed air as propellant gas, injecting radially downstream powder particles near the throat, and reaching lower particle velocities than HPCS of 350–700 m/s [1–3, 15]. Since powder particles injected in LPCS do not flow through the nozzle throat, the nozzle walls wear occurs at the diverging part of the nozzle, ensuring a longer service nozzle life. Table 1 displays the most important differences between HPCS and LPCS [3].

Table 1 Principal characteristics of HPCS and LPCS [8]

Process variable	HPCS	LPCS
Carrier gas	N_2, He or a mixture of both	Air (N_2, He)
Gas pressure (bar)	10–50	6–10
Gas temperature (°C)	800–1000	200–650
Feeding powder rate ($Kg \cdot h^{-1}$)	4.5–13.5	0.3–3
Standoff distance (mm)	10–50	5–15
Particle size (μm)	1–50	5–30
Particle velocities (m/s)	200–1200	350–700

Compared with the HPCS system, LPCS has other advantages including better flexibility and portability, a significant reduction in spraying costs, lower power consumption, and extended nozzle service life. These make LPCS simpler, and safer and allow the use of the equipment at small plants and repair shops. However, it can only attain deposition efficiency below 50%, whereas, HPCS can achieve up to 90% [2, 7, 16, 17]. The common problems associated with LPCS are related to increasing DE, productivity, and spraying harder materials [1, 3, 18].

Several patented nozzle geometries for Cold spraying can be found [17, 19–21], where length has been reported as a primary geometry variable for influencing particle velocity, leaving the nozzle shape as a less responsive variable [22]. Nozzle improvements look for enhancing operating capabilities by increasing spraying area, making smaller apparatus sizing, and enlarging deposition efficiency by rising particle temperature throughout gas flow deceleration after reaching the supersonic region, among others.

Even though coating properties quite depend on the process variables combination, the proper characteristics of the powder such as purity, morphology, particle size, and size distribution, increase the powder ductility and deformability, improving the feasibility of coating in the cold spraying processes [13, 18]. In that regard, copper is an ideal material for spraying and it can be used as based material to isolate process variables in LPCS. Also, the aluminum alloy Al6061 as substrate displays good corrosion and mechanical properties, and it is commonly used in several industries, making it readily available and affordable. Thus, the deposition of Cu over aluminum alloys, like aluminum Al6061, is a well-known substrate-particle system previously reported [2]. Therefore, this system was used to provide reproducibility and reliability of the statistical methodologies used in this work into the mathematical model that links the input and output parameters of the LPCS process.

As mentioned before, LPCS is a low-temperature technique suitable for temperature-sensitive materials. This coating technology feature has opened the opportunity to deposit several composite materials creating a wide variety

of new materials systems to achieve multifunctional surfaces with superior properties to reach the increasing day-to-day aerospace and automotive demands. According to Moridi et al. [23], materials systems where the cold spraying techniques have optimistic potential are ceramics, polymers, nanostructured powders, and finally nonmetallic substrates [24]. The surface metallization process of polymers and polymer matrix composites (PMCs) [25] has improved several properties, such as electrical and thermal conductivity. LPCS system characteristics have also allowed the addition of ceramic particles to the powder metallic particles to rid nozzle clogging, triggering the sprayed surface by removing undesirable particles and reinforcing the coating structure [26].

CGDS processes have not yet reached a mature technology level and they still offer vast fundamental challenges to solve regarding operational parameters key. Even currently, the optimal CGDS operational parameters are acquired from experimentation trials, reviewing existing data, and numerical simulation, among others [1, 2, 27]. Therefore, it is a difficult task to select LPCS operational process parameters selection as these show strong interdependences among them. Since the experimental investigation regarding process optimization of the LPCS process is bounded by the effort in measurement and the high input processing costs, this has encouraged the growth and development of analytical and numerical models for research and industrial applications. There have been published a few works related to input and output process parameters of copper coatings fabricated using the LPCS process to obtain a mathematical model [28–33]; however, most of the prior studies have focused on the HPCS process [18, 34].

The desirable characteristics of obtained coatings by LPCS require a strategy that could help to handle the input variables and provide an empirical relation to depicting the optimal setting of process variables concerning the responses. The LPCS process optimization for single-response and multi-response has been carried out, mainly with the Taguchi method [28, 30], and the utility concept coupled with the Taguchi method [35], where the derivation of the equivalent objective function has been in debate due to the priority of weights to different responses. Other researchers have evaluated the quality and properties of coatings such as thickness, density, and rugosity surface in the function of different input processing parameters. These parameters mainly are the temperature, pressure, type of the working gas, the size distribution of powder particles injected, stand-off distance, and nozzle type among others [28, 29, 31, 33, 35].

In the present research, the response to the output variables (i.e., porosity percentage and thickness coatings, and deposition efficiency) have been measured to develop a descriptive and inferential statistical model. A multivariate analysis of variance, as well as factor analysis, and principal component analysis based on applied mathematics for the acquired data from experimental results for two different nozzle geometries, was elaborated. This model enables correlating the input process parameters such as nozzle type, standoff distance, and the in-flight particle velocity before substrate impact, with the output process parameters for copper coatings fabricated using the LPCS process such as porosity, thickness, and deposition efficiency. This enables obtaining a practical industrial applications comprehensive model for understanding the effect of the input process parameters on the output and final properties of the coatings obtained, which is highly helpful in the selection parameters in the LPCS process, costs, and associated efficiency.

2 Experimental and method procedures

2.1 Experimental LPCS coating procedure

LPCS coatings were prepared by using copper powder Praxair CU-159 99.9%Cu deposited on grit-blasted aluminum alloy 6061 substrates, taking advantage of this well-known reported substrate-particle system [2]. Powder particle size distribution was $-20+6$ μm (i.e., D10 = 6 μm, D50 = 12 μm, and D90 = 20 μm). Powder size distribution was analyzed with a dry dispersion and laser diffraction set-up model HELOS/BR (OM). Aluminum alloy 6061 $23 \times 24 \times 3$ mm substrates were polished and cleansed by an ultra-sonic bath. Coatings were deposited by a DYMET D423 LPCS system. Two different commercial nozzles were used, as can be seen in Fig. 1a, which their main differences are cross-sectional, expansion ratio, and diverging and converging section lengths. Table 2 shows geometrical nozzle features.

Air was used as propellant gas to accelerate the powder particles which were injected radially shortly after the divergent part of the nozzle. Also, the cold spray gun was manipulated with a 6-axis robot (KUKA GmbH) at 0° spray angle and 10 mm/s transverse speed, and a substrate temperature of 200° C. Furthermore, all the above parameters were held constant throughout the sample fabrication. The fixed experimental conditions used are summarized in Table 3, as well as the variable process parameters. Particle in-flight velocity jet before the substrate impact was evaluated by using HiWatch system diagnostic device (Oseir), which is SprayWatch connected with a diode laser as a backlight for the spray jet illumination in the measured area [36]. The experimental setup schematic is depicted in Fig. 1b. The coatings copper deposited were cross-sectioned and metallographically polished up to 4000 SiC grit, after the polishing the samples were electropolished by 10 s to eliminate all the scratches due to the grit. Coating morphologies and

Fig. 1 a Nozzles round and rectangular, **b** schematic arrangement of cold spray accoupled with HiWatch system
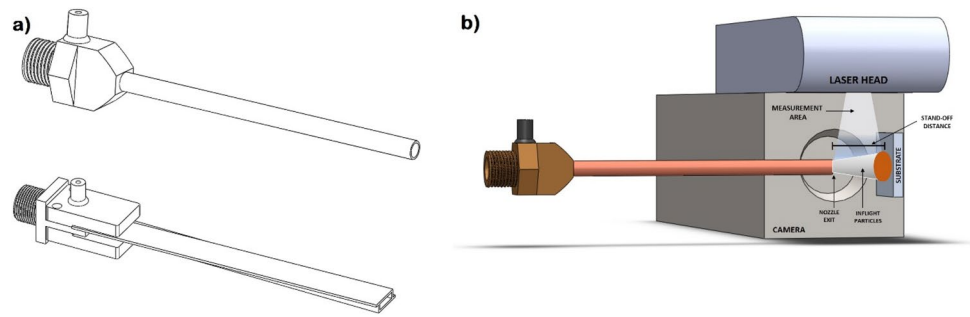
Table 2 Nozzle dimensions

Nozzle type	Throat length (mm)	Exit area (mm^2)	Expansion ratio	Convergent length (mm)	Divergent length (mm)
Round nozzle	7.5	18.1	3.68	11	120
Rectangular nozzle	9.3	31.5	6.4	15	140

Table 3 Process parameters and their values

Fixed process parameter	Value
Stagnation pressure (bar)	8
Stagnation temperature (°C)	600
Traverse speed (m/min)	0.6
Number of layers	3
Powder feeding rate (g/s)	0.25
Substrate temperature (° C)	200
Gas flow rate (m^3/h)	24
Variable process parameter	Value
Stand-off distance (mm)	12.5 and 22.5
Nozzle geometry	Flat and round

microstructures were characterized using a 20X-5000X magnification 970F Keyence optical microscope. The porosity percentage and thickness of coatings were assessed using the ImageJ software analyzer [37, 38]. The porosity percentage was evaluated without any difficulty since the color contrast was very sharp due to excellent polishing.

2.2 Multivariate, factor, and component analysis procedures

This work employed descriptive and inferential statistics to understand the acquired data from the experimental results of porosity, thickness, and deposition efficiency (DE) of the obtained coatings as a function of nozzle type, standoff distance (SOD), and the particle in-flight velocity before the impact of the substrate. Statistical analyses were performed with NCSS 12 Statistical Software, 2018 [39]. The MANOVA methodology was used to deal with the hypothesis concerning a comparison of vectors from group means. Same to the analysis of variance (ANOVA), this method relies on approximations based on the *F*-distribution [40].

The following assumptions were considered for the inferential MANOVA procedure: (a) the response variables were continuous, (b) the residuals accurately follow the multivariate-normal probability distribution with means equal to zero, (c) the variance–covariance matrices of each group residuals are equal, and finally, (d) the individuals are independent [39, 40].

The employed test statistics in this research work for the MANOVA methodology rely on an approximation based on the *F*-distribution as follows. For the case of Wilks' Lambda, the ensuing approximation based on the *F*-distribution was employed to establish the levels of significance [40, 41]:

$$F = \frac{(1 - \Lambda^{\frac{1}{t}})df_2}{\Lambda^{\frac{1}{t}}df_1} \tag{1}$$

where *F* is statistics, *Λ* for Wilk's Lambda test statistic, where matrices are $p \times p$, and the matrix is min (p, vh), here *vh* stands for degrees of freedom associated with the hypothesis and *p* is the number of columns.

Then, $df_1 = pvh$ and $df_2 = wt + 1 - \frac{pvh}{2}$
where,

$$w = ve + vh - \frac{(p + vh + 1)}{2} \tag{2}$$

Hence, *ve* stands for the error degrees of freedom.

Finally,

$$t = \begin{cases} \sqrt{\frac{p^2vh^2-4}{p^2+vh^2-5}} & if \ p^2 + vh^2 - 5 > 0 \\ 1 & \text{otherwise} \end{cases} \tag{3}$$

This means that t is set to one if the numerator or the denominator equals zero. This approach is exact if p or $vh \geq 2$. This approximation was considered based on Tabachnik [40] since Wilk's Lambda largest root is often more powerful if $vh > 1$ and once dimension regards most of the separation between groups.

The factor analysis is used to describe and infer the correlation among predictors as well as response variables, which is an analyzing technique related to a set of noted variables, whose main aim is to find a subset of variables or underlying factors related to the source of the generated observed variables [40].

The partition of the correlation matrix was assumed as follows [40]:

$$R = AA^{\cdot} + U \qquad (4)$$

Hence, the principal axis method is as follows:

1. The estimation of U from the communalities
2. The L and V and the eigenvalues and eigenvectors must be obtained using the analysis of the standard eigenvalues.
3. The calculation of the loading matrix.
4. The calculation of the score matrix and factor scores.

The required communalities for the estimation of U are described below.

$$c_{ii} = \left(1 - \frac{1}{R^{ii}}\right) \frac{\sum_{k=1 \, over \, j \neq k}^{p} \max(|r_{jk}|)}{\sum_{k=1}^{p} \left(1 - \frac{1}{R^{kk}}\right)} \qquad (5)$$

where R_{ii} is the ith diagonal element of $R-1$ and r_{jk} is an element of R. The value of U is then computed by $1-C_{ii}$.

In this factor analysis, the varimax rotation was utilized, due to it being the most common orthogonal rotation technique, where the axes are rotated to maximize the sum of variances of the squared loadings within each column of the loading matrix. Then, let the matrix $G = \{g_{ij}\}$ depict the rotated factors. The varimax rotation aims to maximize the quantity [40]:

$$Q_1 = \sum_{j=1}^{k} \left(\frac{p \sum_{i=1}^{p} g_{ij}^4 - \sum_{i=1}^{p} g_{ij}^2}{p} \right) \qquad (6)$$

How to interpret the data analytics results, such as the case for the MANOVA methodology is very important, since the F-ratio alongside the probability level, helps to determine if the regression model provides an accurate fit to the data than a model that contains non-independent variables. Let us easily explain the interpretation process to infer the quality of the obtained model. Firstly, the probability level obtained for each of the F-ratio values in the MANOVA table must be compared to the significance level, commonly set to 0.05 or 5%, considering a 95% confidence interval upper and lower limits. Hence, if the probability level is below 0.005, the sample data provide sufficient evidence to conclude that the obtained regression model accurately describes the data behavior [42].

The above indicates that the independent variables improve the fit, inferring that these variables statistically influence the measured response. Then, once it has been found that the independent variables considered in the models influence the response, it is time to revise the F-ratio. A higher F-ratio comparison among all the independent variables may help identify the independent variables that greatly affect the measured response, which helps optimize input variables in process control to simplify the process practically.

3 Results and discussion

As stated in the 2.2 subsection, the factor and principal components analysis were performed to describe and infer the correlation among predictors as well as response variables (Table 4), this helps to avoid abstract conclusions obtained from the observer due to the human factor. The normalized code has been established as follows: values closer to zero, represent no correlation, while values closer to 0.30, 0.70–0.80, and 0.90 indicate a low, average, and high correlation, respectively.

Table 4 Scaled principal components heat map

	Nozzle	Standoff	Particle velocity	Porosity	Thickness	Efficiency
Nozzle	1.000	0.062	−0.317	−0.738	0.976	0.896
Standoff	0.062	1.000	−0.843	−0.420	−0.046	−0.002
Particle velocity	−0.317	−0.843	1.000	0.777	−0.153	−0.264
Porosity	−0.738	−0.420	0.777	1.000	−0.602	−0.667
Thickness	0.976	−0.046	−0.153	−0.602	1.000	0.921
Efficiency	0.896	−0.002	−0.264	−0.667	0.921	1.000

Phi = 0.613870 Prob = 0.000002

It is important to mention that factor correlation and principal component procedures were performed. Furthermore, the obtained results were similar for both analyses, hence only principal component results were presented, due to principal component analysis simplifies the interrelated observed variables to a reduced set of important independent composite variables, in contrast to factor correlation where clearly it is assumed the existence of latent factors underlying the observed data. As can be observed in Table 4, the porosity percentage exhibits an average correlation to the process predictors, being more significative than the particle in-flight velocity before impact. This conclusion has been also reported by Zahiri et al. [43], who found that a higher particle in-flight velocity means larger kinetic energy and bigger plastic deformation of particles injected, allowing the removal of voids produced by the cold spraying process obtaining lower porosity levels.

According to the results, it was demonstrated through the analysis that there is a high effect of the nozzle type on the thickness. These results are in good agreement with Fukumoto et al. [44], where it was shown that the nozzle design optimization must improve thickness coating and deposition efficiency. Also, Li et al. [45] found that the nozzle design influences particle velocity and temperature. They also confirmed the feasibility of depositing thicker coatings under a lower gas flow rate, reducing process costs. In this study, the rectangular nozzle presented a decrement of the in-flight particle velocity before the impact of 38% when the standoff distance doubled, meanwhile the round nozzle showed only a decrease of 15%, which denotes the importance of the geometrical features over the particle in-flight velocity.

The deposition efficiency (DE) is strongly dependent on the nozzle type, where the geometry has a significant role in the solid–gas interactions, which can considerably diminish the particle speed at the nozzle exit having a crucial influence on the DE [46]. Both statistical methodologies used in this work (factor and principal components analysis) provided similar results, and a Phi value close to 0.65. This indicates a good correlation between predictors and responses, hence no further correlational analysis was required.

Continuing with the proper discussion of results related to the multivariate analysis, Tables 5 and 6 show the analysis of variance results. Concerning the porosity findings by other authors, Zahiri et al. [43] stated that particle temperature and velocity are the most important input variables to control porosity levels coating. They found a correlation for porosity percentage strongly dependent on temperature and velocity particle aside from mechanical properties of the particles. Moreno et al. [31] found that decreasing powder feeding rate decreases porosity levels and DE, which agrees with the results obtained in this study. It is also reported LPCS process gas temperatures are almost as high as the HPCS process; nevertheless, particles remain for less time in the preheated gas flow because of radially downstream feeding [36]. Usually, particle velocity and temperature are higher in the upstream powder injection systems than in downstream injection systems. Koivuluoto et al. [47] reported a lower mean particle velocity for spraying copper with a similar particle size to this study at 6 bar pressure, 540 °C (60 °C less than this study), and a standoff distance of 10 mm.

As mentioned above, geometrical nozzle features are decisive for determining particle temperature and velocity behavior. The standoff distance directly influences coating porosity because, at a narrow standoff distance, the particles do not develop adequate critical velocity to adhere to the substrate. In conclusion, the particle in-flight velocity is crucial to reaching the necessary deformation for porosity decrease in the LPCS coatings [48]. Hence, the results obtained by the MANOVA methodology point toward the

Table 5 Analysis of variance (porosity) with significance at 95%, where DOF is the degrees of freedom and F-ratio is the value of the F statistic

Source	DOF	Sum of squares	Mean squares	F-ratio	Prob. level
A: Nozzle type	1	40.14	40.14	14.78	0.61
B: Standoff distance	1	0.10	0.10	0.04	0.862
C: Particle in-flight velocity	3	0.15	18.36	6.12	2.250
S	2	5.43	2.71		
Total	7	78.59			

Table 6 Analysis of variance (thickness) with significance at 95%, where DOF is the degrees of freedom and F-ratio is the value of the F statistic

Source	DOF	Sum of squares	Mean squares	F-ratio	Prob. level
A: Nozzle type	1	93610.75	93610.75	158.41	0.006
B: Standoff distance	1	12.93	12.93	0.02	0.896
C: Particle in-flight velocity	2	0.10	2065.51	688.5	1.170
S	7	1181.89	590.93		
Total	8	98487.27			

high dependency of the porosity percentage to the nozzle type, rather than the standoff distance or the particle in-flight velocity before impact, as Table 5 displays. Consequently, it is a matter of great importance to choose the right nozzle design cautiously to improve the quality of the obtained coatings.

As mentioned above, the nozzle type influences the coating porosity level, since the probability level is close to the 0.05 significance level of alpha, indicating a 95% confidence interval, and showing a statistical Fisher's value of 14.78 compared to the F-ratio values overly low for standoff distance and particle in-flight velocity before impact. Figure 2 confirms the conclusion, where is depicted the relatively low percent porosity beneath 6%. Figure 2 also shows the relationship between the particle in-flight velocity and porosity percentage. This is an important consideration for further optimization of the process; Meyer et al. [49] have reported that the feeding rate particle has noticeable importance on the particle dynamics changing particle velocities and influencing the global cold spraying process, and at last, in the final properties of the coating.

Analyzing the thickness through the MANOVA methodology, the following interesting findings can be remarked on. In Table 6, something compelling can be observed, the nozzle type has a value lower than 0.05 significance level, hence conferring reproducibility of the measurements between 95% confidence interval. At this point, it is possible to state that the thickness depends on the nozzle type. However, the F-ratio for the particle in-flight velocity is higher than the nozzle type, indicating a strong effect of the particle in-flight velocity on thickness. Though this conclusion has a drawback, since the probability level is too high compared to the 0.05 significance level, indicating poor reproducibility, discarding this predictor as statistically significant. Regardless, the F-ratio value suggests further research must be conducted to clearly understand the role of the particle in-flight velocity over the coating thickness. Furthermore, the particle in-flight velocity values reported here are higher than those reported in other studies [31], which could be associated with the bounce-off particle effect interfering with in-flight particle velocity measurements.

Again, as in the MANOVA porosity results, the nozzle types affect significative the thickness of the coating, as can be seen in Fig. 3. This has also been reported by Sakaki [50], where it was found that the coating obtained by the rectangular nozzle was flatter and more uniform than the coating obtained by the round nozzle for the HPCS process. Here, the rectangular nozzle has an expansion ratio higher than the round nozzle: 6.4 and 3.68, respectively, and the greater thickness and lower porosity coatings were obtained with the round nozzle. Meanwhile, the rectangular nozzle produced coatings with uppermost porosity and less thickness. Moreover, Fig. 3 illustrates that the standoff distance has no appreciable effect on the resulting thickness since the shock effect has been minimized, which is in good agreement with the study previously reported [31].

Finally, although the particle in-flight velocity results are not conclusive, in Fig. 3, a directly proportional relation between thickness and particle in-flight velocity can be seen. It can also be remarked that the highest particle in-flight velocity is obtained at the shortest stand-off distances, where the rectangular nozzle presents a decrease of 39% when increasing the SOD from 12.5 to 22.5 mm, whereas the round nozzle only decreases 16% the particle in-flight velocity. Therefore, the influence of the particle in-flight velocity on the thickness has a more substantial contribution in the rectangular nozzle than in the round one.

Figure 4 on the left shows the value thickness (μm) of the copper coatings obtained for the rectangular and round nozzles at 12.5 and 22.5 mm of SOD, where it is clear the particle in-flight velocity contribution on the thickness in the rectangular nozzle. Meanwhile, Fig. 4 on the
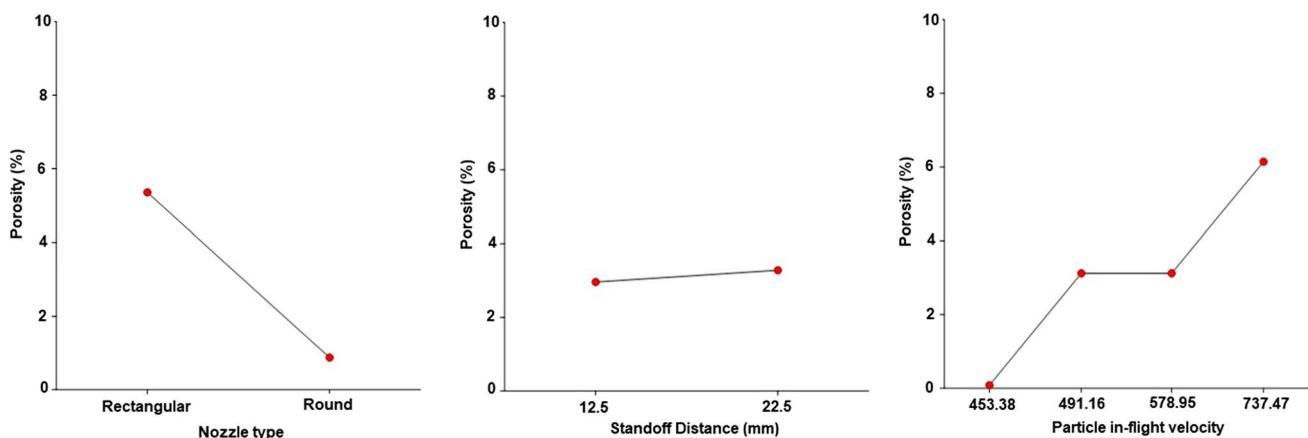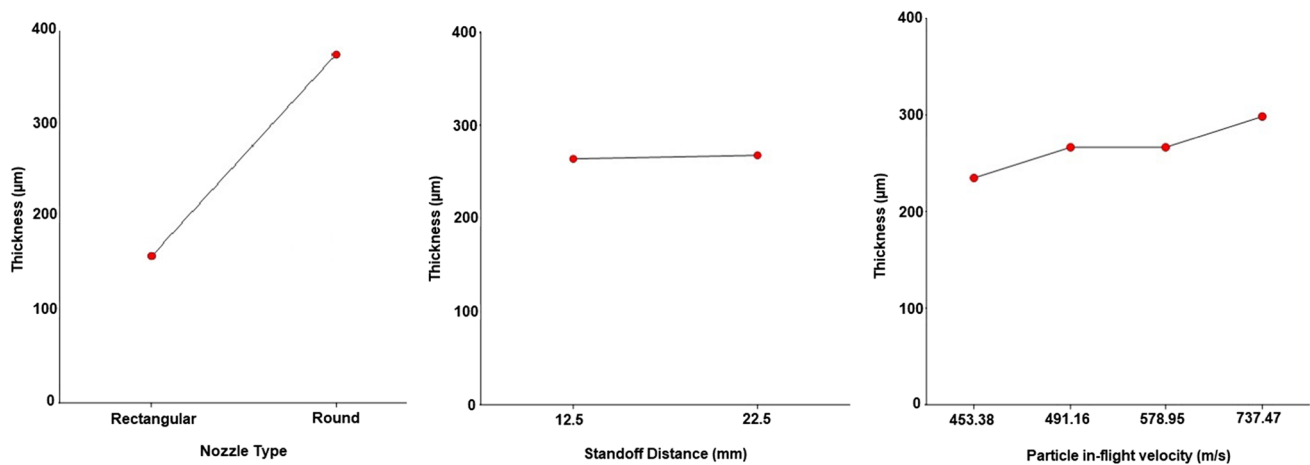

Fig. 2 Effect of nozzle type, standoff distance, and particle in-flight velocity on porosity level

Fig. 3 Effect of nozzle type, standoff distance, and particle in-flight velocity on coating thickness

Fig. 4 Left. Values thickness (μm) of LPCS Cu coatings for rectangular and round nozzles at SOD of 12.5 mm and 22.5 mm. Right. Thickness coatings cross-section for **a**) rectangular nozzle, and **b**) round nozzle
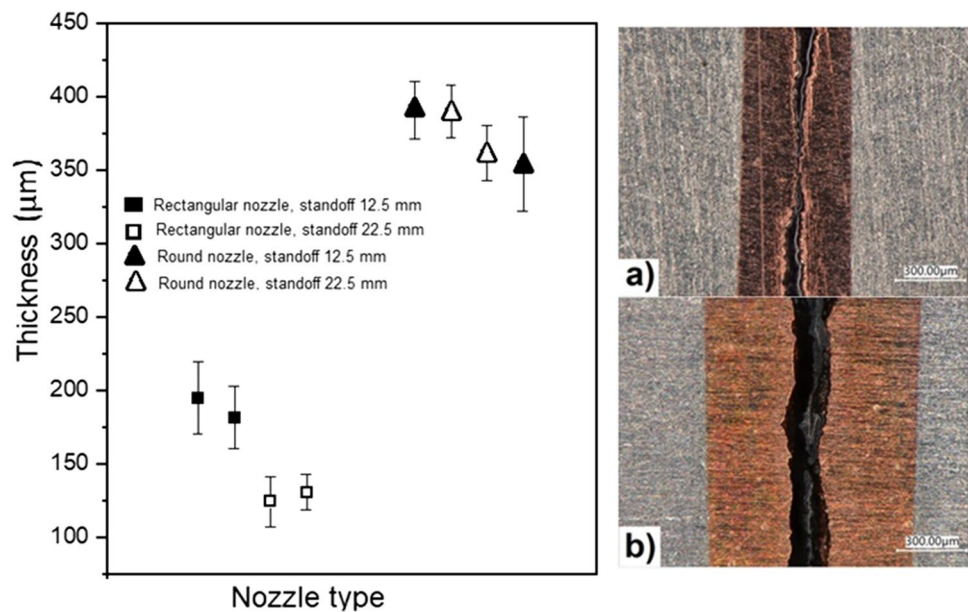

right displays the thickness coatings cross-section for both nozzles, where the thickness differences between both nozzles can be seen at a macroscopic level. Figure 5 exhibits the cross-sectional structures of LPCS copper coatings for both nozzles where it is possible to see the thickness difference and the contributions of both nozzle geometries to the thickness and microstructural characteristics of the coatings with particles deformed shapes highly flattened. Since the difference in the particle in-flight velocity shown for both nozzles has a considerable difference in the function of SOD, it can be assumed that kinetic energy is also different for both. Particle deposition strongly depends on particle in-flight velocity, properties of the substrate, and particles. It can also be concluded that particle in-flight velocity far exceeds the required critical velocity to achieve deposition [33]. This enables a higher coating densification for the rectangular nozzle showing the maximum thickness but the highest coating porosity for the lowest stand-off distance at the highest particle in-flight velocity. Meanwhile, the round nozzle displays moderate particle in-flight velocity, still even upper than the critical velocity value, reaching the highest deposition efficiency (DE) and the lowest coating porosity percent [10, 51].

Finally, Figs. 6, 7, and 8 display the response surface plots of porosity, thickness, and deposition efficiency obtained by applying a statistical modeling methodology previously reported by the research group and that can be consulted elsewhere [52]. These response surface plots are preliminary obtained models that can be used for design or optimization purposes based on the experimental results obtained.

Fig. 5 The cross-sectional structure of LPCS Cu coatings for rectangular nozzle **a**) SOD of 12.5 mm, **b**) SOD of 22.5 mm, and round nozzle, **c**) SOD 12.5 mm, and **d**) SOD of 22.5 mm
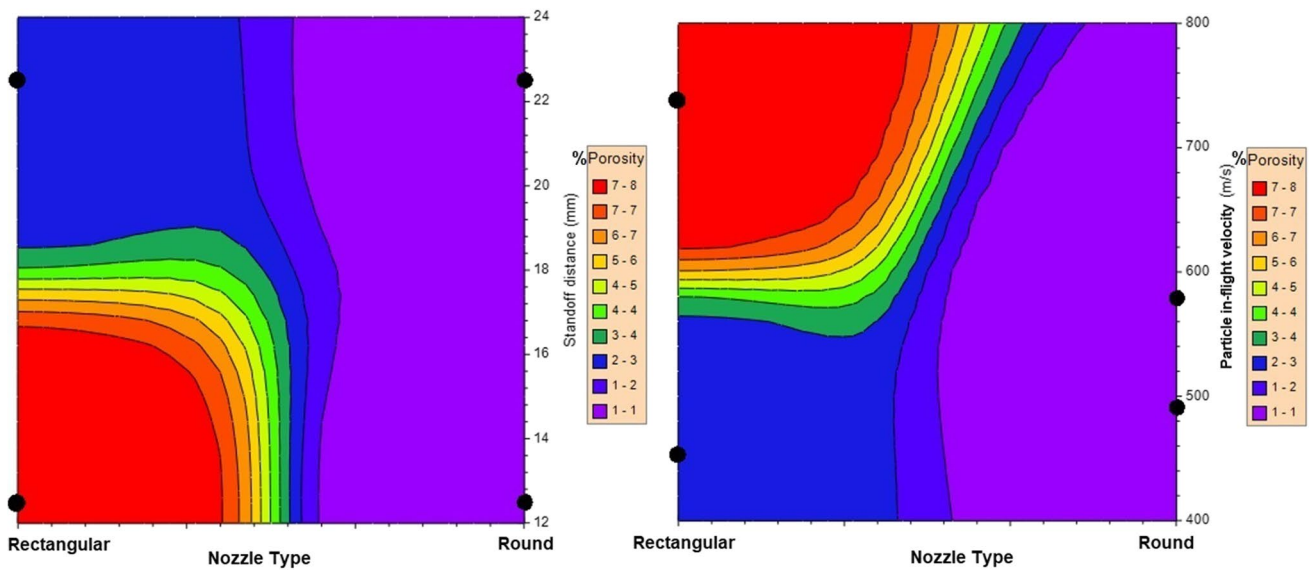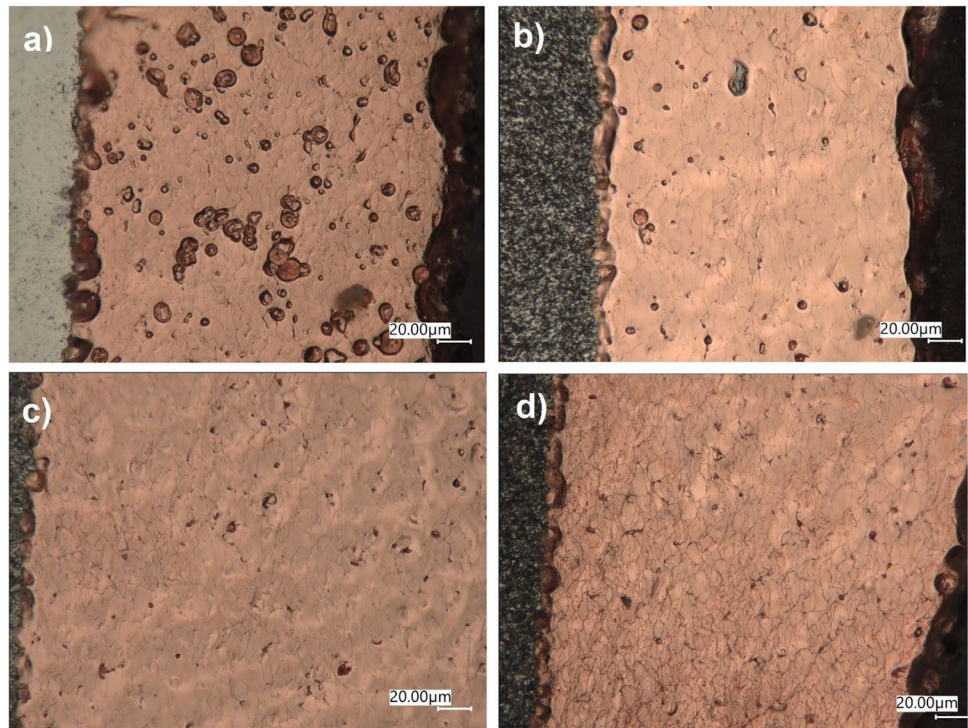
Fig. 6 Response surface plot of porosity vs nozzle type, standoff distance (left), and particle in-flight velocity (right)

Figure 6 indicates that the round nozzle type is recommended for obtaining coatings with low porosity levels. It can also be concluded that this nozzle type enables almost any combination of standoff distance and particle in-flight velocity before impact. Therefore, the selection of these two parameters will be influenced by other decision factors. These conclusions have also been reported previously [45, 53]. However, these findings lack proper statistical and modeling methodologies to ensure the inferences are free from subjective points of view related to the human factor. It should be remarked that no factor affects nozzle performance more than nozzle geometry itself. Nozzle design should guarantee the particle acceleration for reaching deposition and withstand the thermal energy transfer effects. Last, the nozzle cross-section defines, in addition to the particle profile on exiting, the gas process consumption.
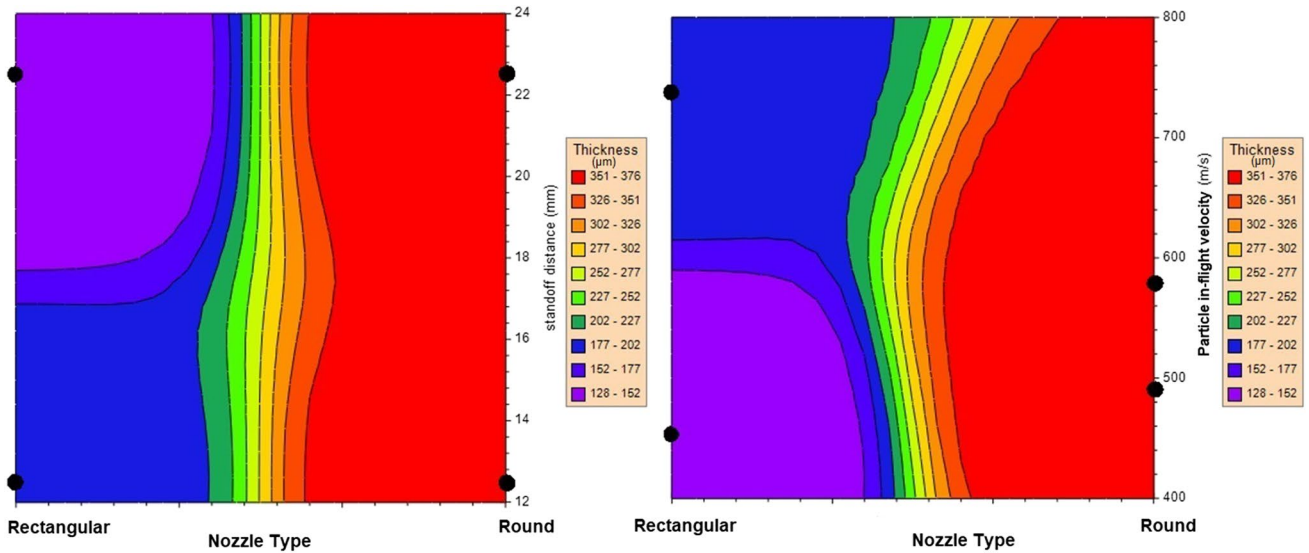
Fig. 7 Response surface plot of thickness vs nozzle type, standoff distance (left), and particle in-flight velocity (right)
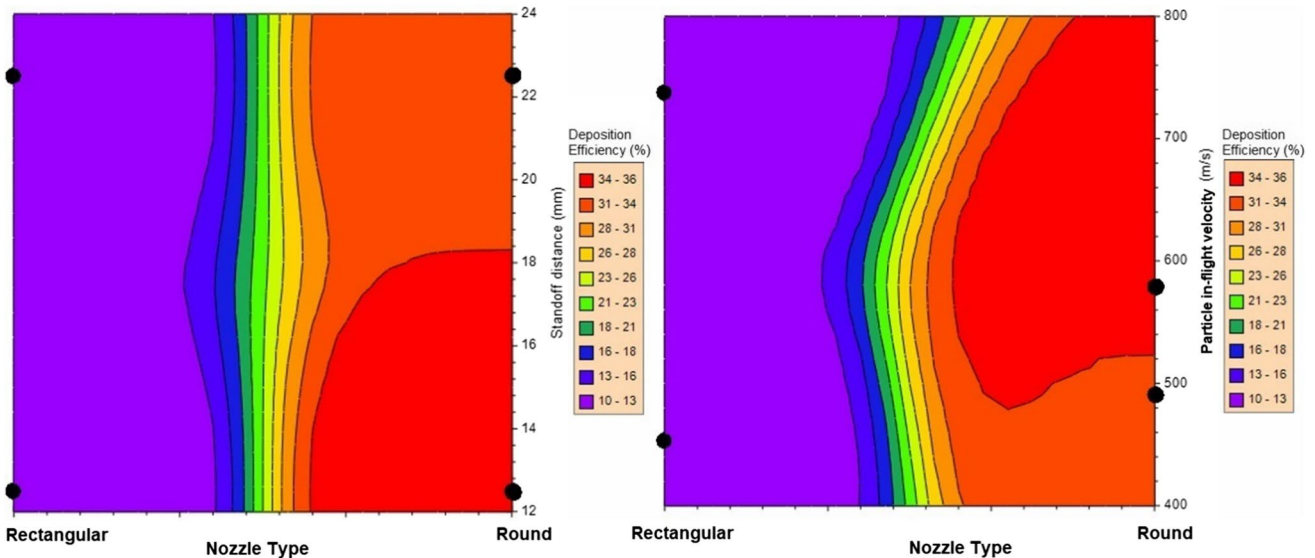

Fig. 8 Response surface plot of deposition efficiency (DE) vs nozzle type, standoff distance (left), and particle in-flight velocity (right)

Consequently, the chosen nozzle geometry should be based on the operational and economic parameters of the process.

When dealing with the optimal parameters to control thickness, it is evident in Fig. 7 that the round nozzle type produces thicker coatings, apparently independent of standoff distance and impact velocity. It could be associated with the round nozzle being 20 mm shorter than the rectangular nozzle in the divergent zone, decreasing the residence time of particles in the gas flow. In addition, the rectangular nozzle shows the largest exit area and a tendency to decrease particle temperature because gas expansion is faster, resulting in its temperature dropping [45].

In Fig. 8 the round nozzle type displayed higher deposition efficiency (DE) levels. However, in contrast to the models shown in Figs. 6 and 7, it is recommended to use standoff distances below 18 mm and particle in-flight velocity before impact above 500 m/s, where this last must be mainly controlled by the nozzle cross-section and the design geometry [10, 45, 51].

Finally, particle in-flight velocity was also considered an output parameter instead of an input parameter in a second statistical analysis to study its dependency on nozzle type and standoff distance. These input variables were those with a strong influence over the coating properties.
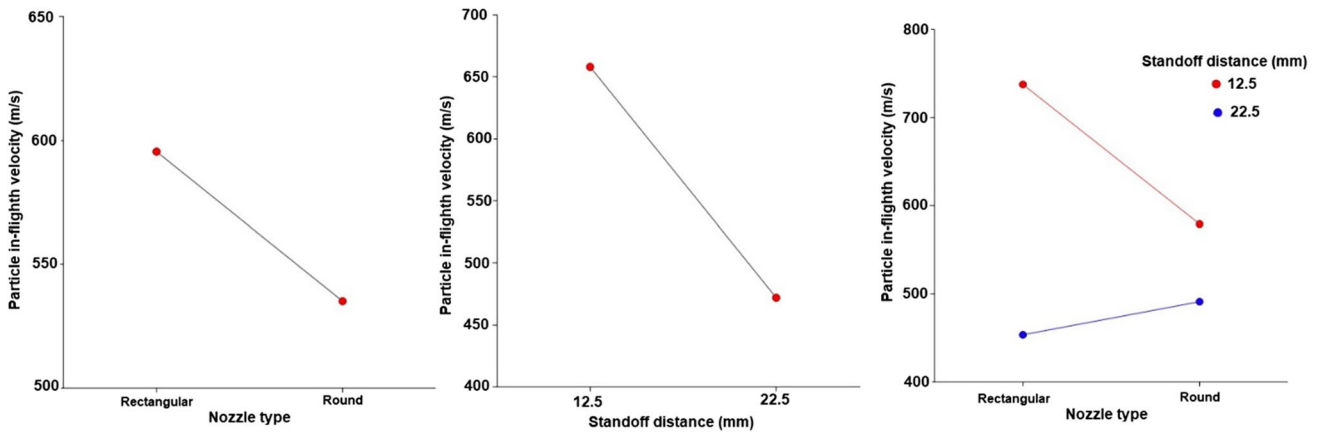
Fig. 9 Effect of nozzle type and standoff distance on particle in-flight velocity

Figure 9 shows the relationship between the particle in-flight velocity, the nozzle type, and the standoff distance. The rectangular nozzle exhibits the highest particle in-flight velocity and the highest velocity increase when the standoff distance doubles. It also presents the highest values of particle in-flight velocity, exceeding the critical particle velocity, producing a high rebound percentage of the particles, and consequently, increasing the porosity of the coating and decreasing its thickness. Figure 10 displays the response surface plot of particle in-flight velocity. Although the round nozzle enlarges discretely the particle in-flight velocity when the standoff increases, this nozzle type is suggested for obtaining coatings with low porosity levels since the particles do not exceed critical velocity in exceeds which is determinant in the final behavior of the particles.

4 Conclusions

This work investigated the acquired data from the LPCS process output variables such as porosity percentage, thickness, and deposition efficiency of the obtained coatings as a function of process input variables, including two nozzle types, two standoff distances, and particle in-flight velocity measures by applying descriptive statistics. Copper powder particles were deposited onto aluminum 6061 substrates. The results obtained are summarized as follows:

1. The Results obtained by the MANOVA methodology highlight a high dependency on the desirable coating properties such as porosity, thickness, and deposition efficiency concerning the geometry of the chosen nozzle.

Fig. 10 Response surface plot of particle in-flight velocity vs nozzle type and standoff distance
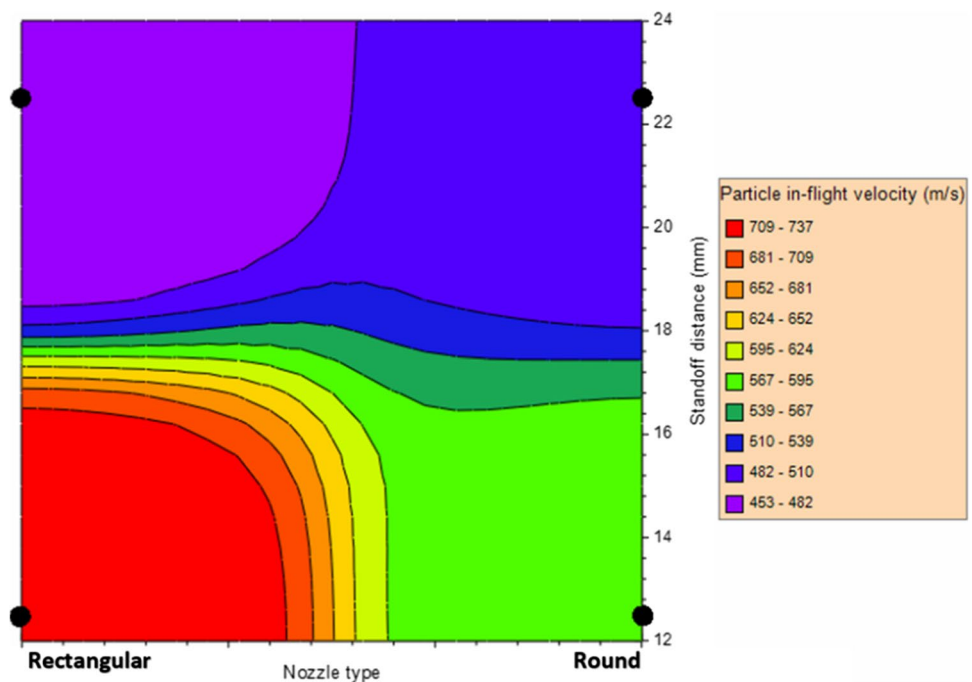
2. Nozzle type affects thickness and deposition efficiency; the rectangular nozzle combined with the largest stand-off distance presented the highest diminution in particle in-flight velocity.

3. The correlation among response variables confirms that thickness is strongly influenced by deposition efficiency.

4. MANOVA methodology also remarks thickness coating dependency with nozzle type within a 95% confidence interval, and a significant particle in-flight velocity contribution being this last predictor statistically irrelevant.

5. Nozzle type greatly influences particle in-flight velocity; in this research, the rectangular nozzle decreases more than twice the particle in-flight velocity with increasing SOD compared with the round nozzle.

6. The highest particle in-flight velocity values for the rectangular nozzle significantly affect deposition efficiency and porosity levels in the coating obtained.

Finally, further work has to be done to pinpoint optimal low-pressure spraying conditions concerning further utilization of statistical methodologies for new substrate/coatings systems since these tools have evidenced profitable industrial applications.

Author contribution All authors contributed to the study's conception and design. Material preparation, data collection, and analysis were performed by Maricruz Hernandez-Hernandez, Rodrigo Gonzalez-Mejia, Victor Hugo Mercado-Lemus, Adriana Gallegos-Melgar, Isabel Pereyra, Juan Muñoz-Saldaña, and Jan Mayen. The first draft of the manuscript was written by Maricruz Hernandez-Hernandez and all authors commented on previous versions of the manuscript. All authors read and approved the final manuscript.

Declarations

Conflict of interest The authors declare no competing interests.

References

1. Srikanth A, Mohammed ThalibBasha G, Venkateshwarlu B (2019) A brief review on cold spray coating process. Mater Today Proc 22:1390–1397. https://doi.org/10.1016/j.matpr.2020.01.482

2. Oyinbo TCJST (2019) A comparative review on cold spray dynamic spraying processes and technologies. Manuf Rev 6:11–13

3. Vuoristo P (2014) Thermal spray coating processes. In: Hashmi S, Batalha GF, Van Tyne CJ, Yilbas BBT-CMP (eds) Elsevier, Oxford, pp 229–276. https://doi.org/10.1016/B978-0-08-096532-1.00407-6

4. Champagne VK (2007) The cold spray materials deposition process: fundamentals and applications. In: Papyrin A (ed) The development of the Cold Spray Process. Woodhead Publishing, Cambridge, pp 11–42. https://doi.org/10.1533/9781845693787

5. Karthikeyan J (2007) The advantages and disadvantages of the cold spray coating process. The cold Spray Materials Deposition Process: Fundamentals and Applications pp 62–71. https://doi.org/10.1533/9781845693787.1.62

6. Ghelichi R, Guagliano M (2009) Coating by the Cold spray process: a state of the art. Frat Ed Integrità Strutt 3:30–44. https://doi.org/10.3221/igf-esis.08.03

7. Singh H, Sidhu TS, Kalsi SBS, Karthikeyan J (2013) Development of cold spray from innovation to emerging future coating technology. J Brazilian Soc Mech Sci Eng 35:231–245. https://doi.org/10.1007/s40430-013-0030-1

8. Champagne VK Jr, Ozdemir OC, Nardi A (2021) Practical cold spray. Springer, Cham. https://doi.org/10.1007/978-3-030-70056-0

9. Dimitris K, Jeandin M, Irissou E, Legoux J-G, Knapp W, Dumitras D (2012) Laser-assisted cold spray (LACS). Nd YAG Laser. IntechOpen, London. https://doi.org/10.5772/36104

10. Maev RG, Leshchynsky (2008) Introduction to low pressure gas dynamic spray: physics and technology, 1st edn. Wiley-VCH, Hoboken

11. Gilmore DL, Dykhuizen RC, Neiser RA, Roemer TJ, Smith MF (1999) Particle velocity and deposition efficiency in the cold spray process. J Therm Spray Technol 8:576–582. https://doi.org/10.1361/105996399770350278

12. Christoulis DK, Guetta S, Guipont V, Jeandin M (2011) The influence of the substrate on the deposition of cold-sprayed titanium: an experimental and numerical study. J Therm Spray Technol 20:523–533. https://doi.org/10.1007/s11666-010-9608-7

13. Stoltenhoff T, Kreye H, Richter HJ (2002) An analysis of the cold spray process and its coatings. J Therm Spray Technol 11:542–550. https://doi.org/10.1361/105996302770348682

14. Li G, Wang XF, Li WY (2007) Effect of different incidence angles on bonding performance in cold spraying. Trans Nonferrous Met Soc China (English Ed.) 17:116–121. https://doi.org/10.1016/S1003-6326(07)60058-2

15. Yin S, Lupoi R (2021) Cold spray additive manufacturing, from fundamentals to applications, Springer Cham. https://doi.org/10.1007/978-3-030-73367-4

16. Winnicki M, Małachowska A, Dudzik G, Rutkowska-Gorczyca M, Marciniak M, Abramski K, Ambroziak A, Pawłowski L (2015) Numerical and experimental analysis of copper particles velocity in low-pressure cold spraying process. Surf Coatings Technol 268:230–240. https://doi.org/10.1016/j.surfcoat.2014.11.059

17. Kashirin AI, Fedorovich K, Valerievich B (2002) Apparatus for gas-dynamic coating, Patent No. US 6402050

18. Koivuluoto H, Coleman A, Murray K, Kearns M, Vuoristo P (2012) High pressure cold sprayed (HPCS) and low pressure cold sprayed (LPCS) coatings prepared from OFHC Cu feedstock: Overview from powder characteristics to coating properties. J Therm Spray Technol 21:1065–1075. https://doi.org/10.1007/s11666-012-9790-x

19. Irissou E, Legoux JG, Ryabinin AN, Jodoin B, Moreau C (2008) Review on cold spray process and technology: Part I - Intellectual property. J Therm Spray Technol 17:495–516. https://doi.org/10.1007/s11666-008-9203-3

20. Guo D, Kazasidis M, Hawkins A, Fan N, Leclerc Z, MacDonald D, Nastic A, Nikbakht R, Ortiz-Fernandez R, Rahmati S, Razavipour M, Richer P, Yin S, Lupoi R, Jodoin B (2022) Cold spray: over 30 years of development toward a hot future. J Therm Spray Technol 31:866–907. https://doi.org/10.1007/s11666-022-01366-4

21. Kashirin AI (2006) Kaluzhskaya Apparatus for gas-dynamic applying coatings and method of coating, European Patent EP 1888803 B1

22. Dykhuizen RC, Smith MF (1998) Gas dynamic principles of cold spray. J Therm Spray Technol 7:205–212. https://doi.org/10.1361/105996398770350945

23. Moridi A, Hassani-Gangaraj SM, Guagliano M, Dao M (2014) Cold spray coating: review of material systems and future perspectives. Surf Eng 30:369–395. https://doi.org/10.1179/1743294414Y.0000000270

24. Viscusi A, Perna AS, Astarita A, Boccarusso L, Caraviello A, Carrino L, Della Gatta R, Durante M, Sansone R (2019) Experimental study of cold sprayed metallic coatings on thermoplastic matrix composites. Key Eng Mater 813:68–73. https://doi.org/10.4028/www.scientific.net/KEM.813.68

25. Della Gatta R, Perna AS, Viscusi A, Pasquino G, Astarita A (2022) Cold spray deposition of metallic coatings on polymers: a review. J Mater Sci 57:27–57. https://doi.org/10.1007/s10853-021-06561-2

26. Koivuluoto H, Vuoristo P (2010) Effect of powder type and composition on structure and mechanical properties of Cu + Al2O3 coatings prepared by using low-pressure cold spray process. J Therm Spray Technol 19:1081–1092. https://doi.org/10.1007/s11666-010-9491-2

27. Oyinbo ST, Jen TC (2019) A comparative review on cold gas dynamic spraying processes and technologies. Manuf Rev 6:11–13. https://doi.org/10.1051/mfreview/2019023

28. Goyal T, Walia RS, Sidhu TS (2012) Study of coating thickness of cold spray process using Taguchi method. Mater Manuf Process 27:185–192. https://doi.org/10.1080/10426914.2011.564249

29. Goyal T, Walia RS, Sidhu TS (2012) Effect of parameters on coating density for cold spray process. Mater Manuf Process 27:193–200. https://doi.org/10.1080/10426914.2011.566906

30. Goyal T, Walia RS, Sidhu TS (2012) Surface roughness optimization of cold-sprayed coatings using Taguchi method. Int J Adv Manuf Technol 60:611–623. https://doi.org/10.1007/s00170-011-3642-6

31. Moreno-Murguia B, Mora-Garcia AG, Canales-Siller H, Giraldo-Betancur AL, Espinosa-Arbelaez DG, Muñoz-Saldaña J (2022) Influence of stand-off distance and pressure in copper coatings deposition efficiency and particle velocity. Surf Coatings Technol 430:1–8. https://doi.org/10.1016/j.surfcoat.2021.127986

32. Singh PK, Tripathi A (2017) CFD Analysis of De-Laval Nozzle, vol 3, issue 2. IJARIIE-ISSN(O)-2395-4396. www.ijariie.com

33. Gärtner F, Stoltenhoff T, Voyer J, Kreye H, Riekehr S, Koçak M (2006) Mechanical properties of cold-sprayed and thermally sprayed copper coatings. Surf Coatings Technol 200:6770–6782. https://doi.org/10.1016/j.surfcoat.2005.10.007

34. Hamweendo A, Popoola P, Botef I (2014) Mathematical model for predicting process parameters in CS of Ti. Mathematical Methods in Science and Engineering, pp 225–229

35. Goyal T, Walia RS, Sidhu TS (2013) Multi-response optimization of low-pressure cold-sprayed coatings through Taguchi method and utility concept. Int J Adv Manuf Technol 64:903–914. https://doi.org/10.1007/s00170-012-4049-8

36. Larjo J, Hämäläinen E, Kriikka N (2003) In-flight particle imaging in thermal spraying with diode laser illumination, Thermal Spray 2003: Proceedings from the International Thermal Spray Conference, Paper No: itsc p1113, pp 1113–1116. https://doi.org/10.31399/asm.cp.itsc2003p1113

37. Schneider CA, Rasband WS, Eliceiri KW (2012) NIH Image to ImageJ: 25 years of image analysis. Nat Methods 9:671–675. https://doi.org/10.1038/nmeth.2089

38. Shi X, Wang Y, Li H, Zhang S, Zhao R, Li G, Zhang R, Sheng Y, Cao S, Zhao Y, Xu L, Zhao Y (2020) Corrosion resistance and biocompatibility of calcium-containing coatings developed in near-neutral solutions containing phytic acid and phosphoric acid on AZ31B alloy. J Alloys Compd 823:153721. https://doi.org/10.1016/j.jallcom.2020.153721

39. NCSS L (2018) NCSS 12, Statistical Software. Kaysville, Utah, USA. ncss.com/software/ncss

40. Fidell L, Tabachnick B (n.d.) Using multivariate statistics, 5th ed. – PsycNET, Allyn & Bacon/Pearson Education, Boston. https://psycnet.apa.org/record/2006-03883-000

41. Rao CR (1951) An asymptotic expansion of the distribution of Wilk's criterion. Bull Int Stat Inst 33:177–180

42. Moore DS, Kirkland, Notz WI (2021) The best practice of statistics, 9th edn. WH Freeman, New York

43. Zahiri SH, Fraser D, Gulizia S, Jahedi M (2006) Effect of processing conditions on porosity formation in cold gas dynamic spraying of copper. J Therm Spray Technol 15:422–430. https://doi.org/10.1361/105996306X124437

44. Fukumoto M, Terada H, Mashiko M, Sato K, Yamada M, Yamaguchi E (2009) Deposition of copper fine particle by cold spray process. Mater Trans 50:1482–1488. https://doi.org/10.2320/matertrans.MRA2008223

45. Li WY, Liao H, Wang HT, Li CJ, Zhang G, Coddet C (2006) Optimal design of a convergent-barrel cold spray nozzle by numerical method. Appl Surf Sci 253:708–713. https://doi.org/10.1016/j.apsusc.2005.12.157

46. Lupoi R (2014) Current design and performance of cold spray nozzles: experimental and numerical observations on deposition efficiency and particle velocity. Surf Eng 30:316–322. https://doi.org/10.1179/1743294413Y.0000000214

47. Koivuluoto H, Matikainen V, Larjo J, Vuoristo P (2018) Novel online diagnostic analysis for in-flight particle properties in cold spraying. J Therm Spray Technol 27:423–432. https://doi.org/10.1007/s11666-018-0685-3

48. Zahiri SH, Antonio CI, Jahedi M (2009) Elimination of porosity in directly fabricated titanium via cold gas dynamic spraying. J Mater Process Technol 209:922–929. https://doi.org/10.1016/J.JMATPROTEC.2008.03.005

49. Meyer M, Yin S, Lupoi R (2017) Particle In-flight velocity and dispersion measurements at increasing particle feed rates in cold spray. J Therm Spray Technol 26:60–70. https://doi.org/10.1007/s11666-016-0496-3

50. Sakaki K (2007) The influence of nozzle design in the cold spray process. In: Champagne VK (ed) The cold spray materials deposition process. Woodhead Publishing, Cambridge. https://doi.org/10.1533/9781845693787.2.117

51. Singh S, Singh Raman RK, Berndt CC, Singh H (2021) Influence of cold spray parameters on bonding mechanisms: A Review. Metals. https://doi.org/10.3390/met11122016

52. Abúndez A, Pereyra I, Campillo B, Serna S, Alcudia E, Molina A, Blanco A, Mayén J (2016) Improvement of ultimate tensile strength by artificial aging and retrogression treatment of aluminum alloy 6061. Mater Sci Eng A 668:201–207. https://doi.org/10.1016/J.MSEA.2016.05.062

53. Papyrin AN (2007) Cold spray technology. In: Papyrin A, Kosarev V, Klinkov S, Alkimov A, Fomin V (eds) Elsevier. https://doi.org/10.1016/B978-008045155-8/50000-4